

Clusters formed by dumbbell-like one-patch particles confined in thin systems

メタデータ	言語: eng 出版者: 公開日: 2021-09-13 キーワード (Ja): キーワード (En): 作成者: メールアドレス: 所属:
URL	https://doi.org/10.24517/00064090

This work is licensed under a Creative Commons Attribution-NonCommercial-ShareAlike 3.0 International License.





OPEN

Clusters formed by dumbbell-like one-patch particles confined in thin systems

Masahide Sato

Performing isothermal-isochoric Monte Carlo simulations, I examine the types of clusters that dumbbell-like one-patch particles form in thin space between two parallel walls, assuming that each particle is synthesized through the merging of two particles, one non-attracting and the other attracting for which, for example, the inter-particle interaction is approximated by the DLVO model. The shape of these dumbbell-like particles is controlled by the ratio of the diameters q of the two spherical particles and by the dimensionless distance l between these centers. Using a modified Kern–Frenkel potential, I examine the dependence of the cluster shape on l and q . Large island-like clusters are created when $q < 1$. With increasing q , the clusters become chain-like. When q increases further, elongated clusters and regular polygonal clusters are created. In the simulations, the cluster shape becomes three-dimensional with increasing l because the thickness of the thin system increases proportionally to l .

Particles having patch areas in which properties are different from those of other surface areas are termed patchy particles. Many groups^{1–24} have synthesized patchy particles using different methods and examined the self-assemblies formed by patchy particles. Because patchy particles are promising building blocks for functional materials, efficient synthetic methods and properties of self-assemblies have been studied intensely. For example, triblock patchy particles having two patches on the polar positions^{3–5,8,23,24} have drawn much attention as building blocks for photonic crystals with a complete photonic band gap^{25,26}. Whereas patchy particles used in experiments were not necessarily spherical^{6,11,16}, the structures and cluster shapes examined in a theoretical study²⁷ and simulations^{28–41} were mainly for spherical patchy particles.

In studies on non-spherical patchy particles, Monte Carlo simulations of dumbbell-like one-patch particles with a modified Kern–Frenkel potential were performed^{42–44}, and the self-assemblies created by such particles were studied. It was shown that several types of clusters such as spherical micelles, elongated micelles, vesicles, and bilayers are created in three-dimensional systems^{42,43} by controlling the shape of the dumbbell-like one-patch particle. When the long axis of such particles is fixed within a flat plane, island-like clusters with voids, mesh-like clusters, and straight chain-like clusters are observed in addition to elongated clusters and isotropic clusters in two-dimensional systems⁴⁴. In previous studies^{42–44}, the attraction length in the modified Kern–Frenkel potential was set to be as long as the radius of the attractive sphere of the dumbbell-like particles. However, in several experiments^{7,9}, the attraction length was revealed to be much smaller than the radius of patchy particles. Because the attraction length in the Kern–Frenkel potential⁴⁵ affects the structure and shape of clusters, even for spherical patchy particles^{36,46–48}, the shape of the clusters formed by dumbbell-like patchy particles probably depends on the attraction length as well.

In this paper, I describe isothermal-isochoric simulations for dumbbell-like patchy particles in thinly confined systems as shown in Fig. 1, in which the attraction length of the modified Kern–Frenkel potential is set shorter than that in previous studies^{42–44}. I examine how cluster types depend on the shapes of dumbbell-like patchy particles. In the simulations, the focus is on the formation of clusters in thin systems because films of high quality are required as substrates for colloidal epitaxy^{39,49–51}. Compared with creating quality three-dimensional functional materials spontaneously in open three-dimensional spaces, creating the desired structures on substrates by epitaxial growth may be easier. The formation of two-dimensional materials and quasi two-dimensional materials is also a popular topic because thin sheet materials are useful in a broad range of applications such as photovoltaics, semiconductors, electrodes, water purification^{52,53}. The types of the two-dimensional clusters and structures that are formed when the long axes of dumbbell-like particles are fixed in a flat plane have already been studied⁴⁴. Different clusters may be created if the dumbbell-like one-patch particles rotate freely three-dimensionally. Under

Emerging Media Initiative, Kanazawa University, Kanazawa 920-1192, Japan. email: msato002@staff.kanazawa-u.ac.jp

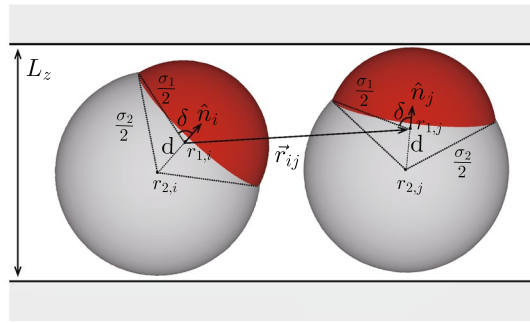


Figure 1. System used in simulations, where dumbbell-like one-patch particles are confined between two flat walls. The particles are synthesized by merging two spheres. Red and white regions represent attractive area and non-attractive area, respectively. The shape of particles is characterized by $q = \sigma_2/\sigma_1$ and $l = 2d/(\sigma_1 + \sigma_2)$, where σ_2 and σ_1 denote the diameters of the non-attractive and attractive spheres, respectively, d the distance between the centers of the two spheres, and l the dimensionless distance scaled by average diameter. δ satisfies $\cos \delta = (\sigma_2^2 - \sigma_1^2 - 4d^2)/4d\sigma_1 = 2l/(1 - q) - (1 + q)l^2$. The particle shape is more dumbbell-like with increasing d . The unit vector directed from the center of the non-attractive sphere to that of the attractive sphere is denoted as \hat{n} . σ_1 is set to unit, and the x - and y -directions are set parallel to the walls, and the z -direction is set perpendicular to the walls, which are given by $z = 0$ and $z = L_z$. With the distance between the two walls denoted by L_z , the lengths of the wall in the x - and y -directions, L_x and L_y , are given by $L_x = L_y = \sqrt{vN/(\rho L_z)}$, where v , ρ , and N denote the volume of the dumbbell-like particle, the particle density, and the number of particles, respectively. The distance between the two walls L_z is set to $1.1[(\sigma_1 + \sigma_2)/2 + d]$. Because L_z is slightly longer than the long axis in the dumbbell-like patchy particles, the particles rotate three-dimensionally.

this scenario, I investigate in the rest of this paper the formation of clusters and structures in thin systems. First, I show several typical snapshots of simulations. Then, I introduce four parameters and show how cluster shapes and structures formed by dumbbell-like patchy particles depend on particle shape.

Results and discussions

Isothermal-isochoric Monte Carlo simulations, performed with number of particles $N = 1024$ and the particle density $\rho = 0.2$ in the system shown in Fig. 1, provided the dataset to examine how cluster shape depends on the shape of dumbbell-like particles.

Typical snapshots for large clusters. Figures 2 and 3 show typical snapshots viewed from the z -direction. The temperature T satisfies $\epsilon/k_B T = 8.0$, where k_B is Boltzmann's constant and ϵ denotes the attractive energy. The zoomed snapshots of the areas surrounded by white circles in each figure are shown in Fig. 4. One large island-like cluster is created when $(l, q) = (0.7, 0.7)$ (see Fig. 2a). Almost all the dumbbell-like patchy particles are connected and included in the island-like cluster. Because σ_2 is smaller than σ_1 , the steric hindrance caused by the non-attractive region is weak when \hat{n} of every particle is perpendicular to the walls. Whereas \hat{n} is almost perpendicular to the walls for the most of particles inside the island-like cluster, \hat{n} for particles located at the edge of the cluster fluctuate because the number of neighboring particles is small. Moreover, the binding of particles at the cluster edge is weak, and therefore the particles at the edge of the island-like cluster rotate easily under thermal fluctuations. In our previous study⁴⁴, a square lattice with voids is created because the interaction length is set to $\sigma_1/2$, and particles at the diagonal positions can attract each other. However, the particles inside the large island-like cluster form a triangular lattice because the attraction length is so short that the particles at diagonal positions cannot interact with each other even if a square lattice is made (Figs. 2b and 4a). The attracting particles are most numerous in a triangular lattice when the interaction length is sufficiently short. With the number of neighbors being six, the energy change per particle is 3ϵ .

Creating large island-like clusters with increasing q or l becomes hard because steric hindrance arising from the non-attractive area in particles increases. The cluster changes from forming islands to forming chains (Fig. 2c and d). In these figures, several particles with six neighbors are seen in places. However, when one particle has six neighbors, \hat{n} of the neighboring particles tilts from the z -direction (see Fig. 4b) because σ_1 is smaller than σ_2 . Therefore, neighboring particles cannot have six connections. Steric hindrance incurred by the non-attractive area suppresses the creation of large island-like clusters, and two-dimensional chain-like clusters consisting of two arrays of dumbbell-like patchy particles form. The particles in perfectly straight chain-like clusters have four connecting neighbors, two neighbors in the same array and in the other array diagonally in front. The energy gain per particle by forming the chain-like clusters is 2ϵ .

Typical snapshots for small clusters. The shape of the dumbbell-like particle becomes more anisotropic with increasing l . The system width L_z increases with increasing l because the system width is set so that the dumbbell-like one-patch particles are able to rotate easily in the thin systems. When $q = 1$ and $l > \sqrt{3}/2$, creating three-dimensional arrays is possible if \hat{n} of each dumbbell-like patchy particle is parallel to the xy -plane. Top and side views of a portion of the three-dimensional arrays are presented in Fig. 4i and j, respectively. When

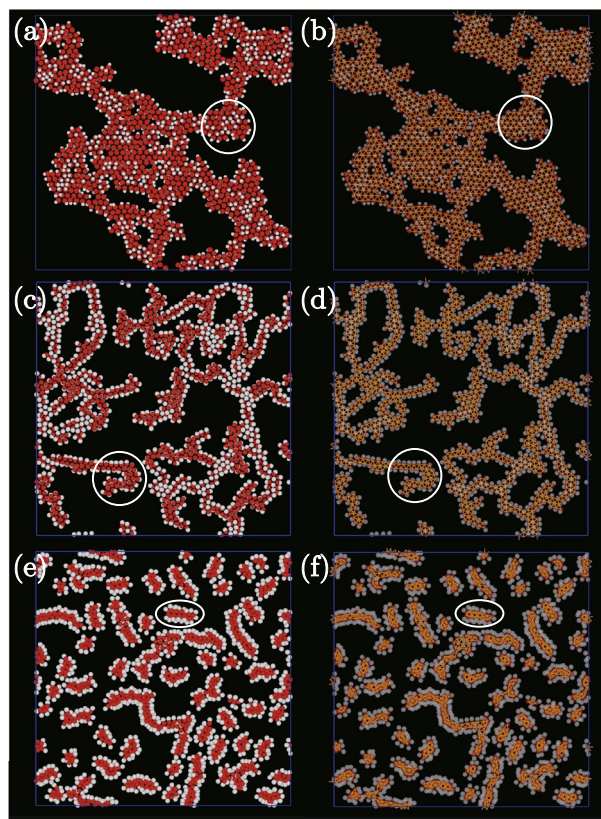


Figure 2. Typical snapshots of large clusters for $\epsilon/k_B T = 8.0$ as viewed from the z -direction. The parameter setting for (l, q) are (a) and (b) (0.70, 0.70), (c) and (d) (0.50, 1.05), and (e) and (f) (0.85, 1.05). Only particle positions are drawn in (a), (c), and (e). The white and red areas show the non-interacting and attracting areas, respectively. In (b), (d), and (f), in addition to the particle positions, attracting particles are connected by lines.

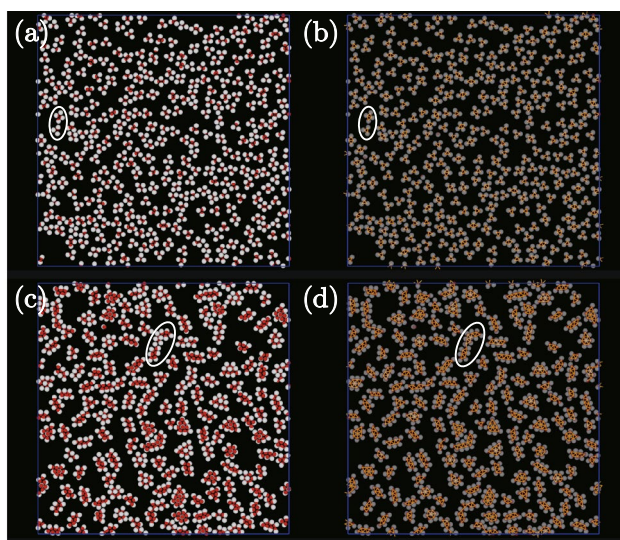


Figure 3. As for Fig. 2 but with (l, q) set to (0.20, 1.25) in (a) and (b), and (0.45, 1.25) in (c) and (d).

the two arrays attract each other and double chain-like clusters form, as in Fig. 4k, each particle in the double chain-like clusters attracts six other particles, their number being the same as the number of neighbors in an island-like cluster. The radius of the non-attractive area in the dumbbell-like patchy particles is larger than that of the attractive part for $q > 1$. Through steric hindrance from the non-attractive sphere, the three-dimensional double chain-like clusters need to be curved (Fig. 4k). With a further decrease in q , the curved chain-like clus-

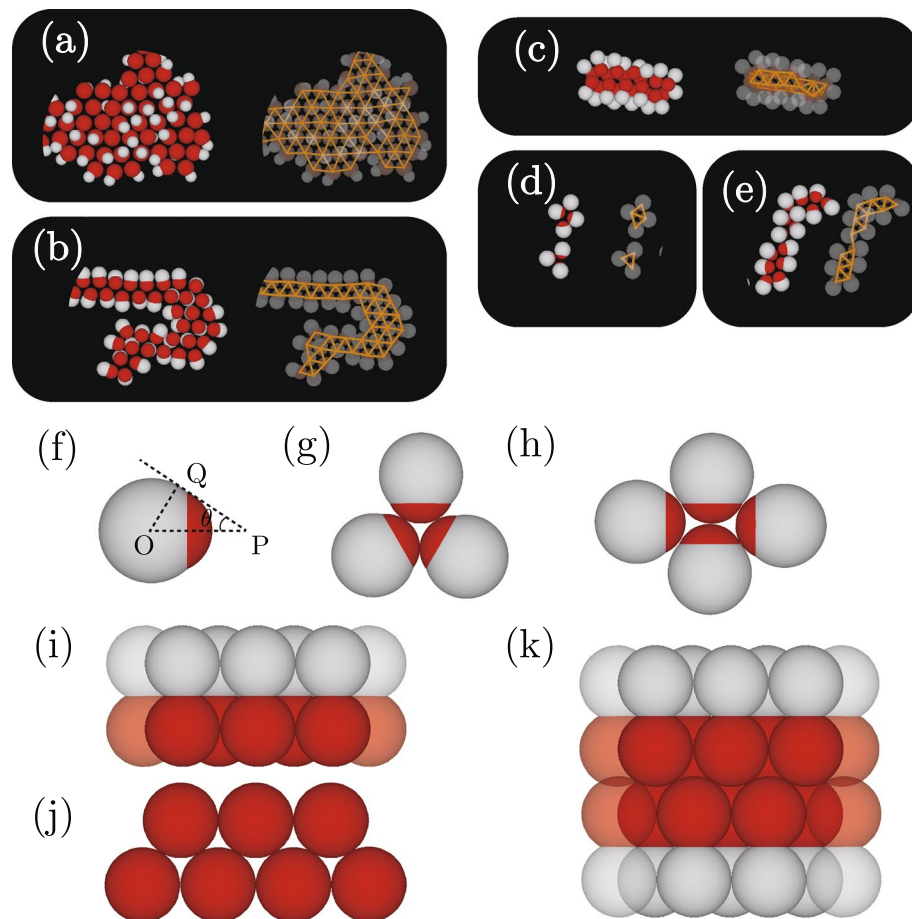


Figure 4. (a–d) Structures and clusters surrounded by circles or ovals in Figs. 2 and 3. The settings for (l, q) are (a) (0.70, 0.70), (b) (0.50, 1.05), (c) (0.85, 1.05), (d) (0.20, 1.25), and (e) (0.45, 1.25). (f) Typical dumbbell-like one-patch particle for a small interaction part, (g) triangular trimer, and (h) square tetramer. (i) Top view and (j) side view of a three-dimensional single array for $q = 1$, and (k) top view of the three-dimensional double chain-like structure formed by two single arrays.

ters are easily torn off creating three-dimensional elongated clusters (Figs. 2e, f and 4c). With q constant and l decreased, instead of the formation of three-dimensional elongated clusters, two-dimensional elongated clusters form (Figs. 3c, d, and 4e).

Typical snapshots for regular clusters. Figure 3a and b show snapshots for small l and large q . Many small two-dimensional polygonal clusters, for example, triangular trimers (Fig. 4g) and rhomboidal tetramers (Fig. 4h) are created (Fig. 4d). The q and l condition for forming triangular trimers is easily estimated. Figure 4f shows the typical shape of a dumbbell-like one-patch particle for which \hat{n} is parallel to the xy -plane; here O labels the center of the non-attractive sphere, and PQ the common tangent of the non-attractive sphere and the attractive sphere that determine angle $\theta = \angle P Q O$ satisfying $\sin \theta = (\sigma_2 - \sigma_1)/2d = (q - 1)/l(q + 1)$. The angle δ (see Fig. 1) needs to be larger than 30° for dumbbell-like patchy particles to create triangular trimers and θ should be smaller than 60° to avoid steric hindrance induced by the non-attractive sphere. The condition for θ is slightly stricter than that for δ when $q > 1$. Therefore, to create triangular trimers, l and q need to satisfy $l > 2(q - 1)/\sqrt{3}(q + 1)$. With $q = 1.25$, l needing to be larger than 0.128 to create triangular trimers, the condition for forming trimers indicated in Figs. 3c and 4d is satisfied. For rhomboidal tetramers, the criterion for avoiding steric hindrance is slightly more complicated to estimate, but that for δ is easier. Because δ is larger than 60° to create rhomboidal tetramers, we obtain the inequality $l > (-1 + \sqrt{4q^2 - 3})/2(1 + q)$. Given l needs to be larger than 0.178 when $q = 1.25$, the condition required in forming rhomboidal tetramers seen in Fig. 3 seems reasonable.

I also examine whether the formation of regular trimers and tetramers obeys the criteria for another q . For $q = 1.6$, the range of l values for which two-dimensional triangular trimers and two-dimensional rhomboidal tetramers are created are estimated to $l > 0.27$ and $l > 0.33$, respectively. Figure 5 shows the cluster size distributions observed from simulations with $\epsilon/k_B T = 8.0$. When $l < 0.30$, almost all particles are monomers although the formation of dimers is allowed, which is probably because the attractive area is too small to make stable dimers with this temperature. With $l = 0.30$, many dimers are created although many monomers still

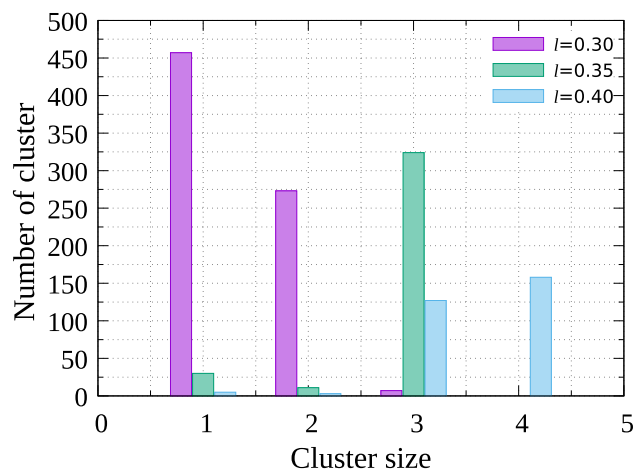


Figure 5. Distribution of cluster size for $(l, q) = (0.3, 1.6)$, $(0.35, 1.6)$, and $(0.4, 1.6)$ with $\epsilon/k_B T = 8.0$.

remain. As expected from the criterion given by the inequality for the formation of trimers, a few trimers are also created. With $l = 0.35$, the main clusters are trimers. Tetramers are not observed, although their formation is expected from the inequality for the formation of tetramers because l is very close to the formation threshold. When $l = 0.4$, tetramers are created because l is above the threshold. Because the energy gain by the formation of two-dimensional tetramers is larger than that of two-dimensional trimers, tetramers are created in higher numbers than trimers.

Classification of cluster types by order parameters. To classify cluster types systematically and to show how the cluster type depends on the particle shape quantitatively, four parameters $P_s = \sum_k k N_k / N^2$, $P_z = \sum_i |n_{zi}| / N$, $\mathcal{M} = (N - N_1)^{-1} \sum_i \hat{n}_i \cdot (\mathbf{r}_{c1} - \mathbf{r}_{1,i}) / |\mathbf{r}_{c1} - \mathbf{r}_{1,i}|$, and $\sigma_z = \sqrt{N^{-1} \sum_i z_{1,i}^2 - (N^{-1} \sum_i z_{1,i})^2}$ are introduced, in which N_k denotes the number of clusters formed by k particles, n_{zi} the z -component of \hat{n}_i , N_1 the number of monomers, $\mathbf{r}_{1,i}$ the center of the attractive sphere of the i -th particle, \mathbf{r}_{c1} the average position of attractive spheres for the cluster including the i -th particle, and $z_{1,i}$ is the z -coordinate of the center of the attractive sphere of the i -th particle. In the definition of \mathcal{M} , the summation does not include monomers.

The l and q dependence of P_s , P_z , σ_z , and \mathcal{M} depend on l and q for $\epsilon/k_B T = 8.0$ were obtained (Fig. 6). P_s is found to be small with $q > 1$ but suddenly increases around $q = 1$ (see Fig. 6a). With $q < 1$, P_s is over 1000, which means that almost all particles in the system are connected and one large cluster is created. Large P_s indicates the formation of large clusters, but I cannot identify whether the cluster type is large island-like or chain-like. From Fig. 2, n_z is large for particles in island-like clusters but small for chain-like clusters. Therefore, P_z is a useful parameter for determining the shape of large clusters. Because P_z is large when both q and l are small (Fig. 6b), large island-like clusters are created in this parameter regime.

The parameter \mathcal{M} is large when regular polygonal clusters form because the direction of every particle points toward the center of a regular polygonal cluster such as triangular trimers and rhomboidal tetramers. \mathcal{M} becomes large for large q and small l (Fig. 6d), which agrees with the formation of triangular trimers and rhomboidal tetramers (Figs. 3a, b and 4d). σ_z is used as a parameter indicating the three-dimensionality of small clusters because the distribution of the z -coordinate of attractive spheres spreads when three-dimensional clusters are created. Therefore, both \mathcal{M} and σ_z are used to determine the shapes of small clusters. The criteria for classifying cluster types are listed in Table 1. Because three-dimensional chain-like clusters are not observed in the simulations, large clusters for which the size is comparable to N are classified into two-dimensional island-like clusters or two-dimensional chain-like clusters. Small clusters are classified into three-dimensional elongated clusters, two-dimensional elongated clusters, or two-dimensional regular clusters. Checks were made as to whether the criteria used for the classification are consistent with snapshots for several sets of l and q ; the criteria were confirmed as reasonable.

Simulations were also performed for $\epsilon/k_B T = 4.0$ and $\epsilon/k_B T = 8.0$ and analyzed to determine whether the dependence of cluster shape on l and q changes with temperature. Figure 7 shows how the cluster type depends on l and q for those temperatures; large island-like clusters form when $q < 1$. The parameter regime yielding island-like clusters is much larger than that yielding chain-like clusters. The width of the latter regime becomes small with decreasing l because steric hindrance exhibits the same trend. I have already suggested that the formation of three-dimensional double chain-like clusters for which the size is comparable to N is possible if $l > \sqrt{3}/2$ for $q = 1$. However, the three-dimensional double chain-like clusters were not created in simulations, probably because the temperatures are high in simulations. The chain-like clusters must be easily broken into three-dimensional elongated clusters through thermal fluctuations arising from higher temperatures. Although the upper limit of l for forming two-dimensional polygonal clusters increases with increasing q , the change in the lower limit of l for the formation of three-dimensional elongated clusters is small. Comparing Fig. 7a with Fig. 7b, when the temperature increases, the two limits move to widen the parameter regime associated with two-dimensional clusters. The boundary between the region with large clusters and that with two-dimensional clusters

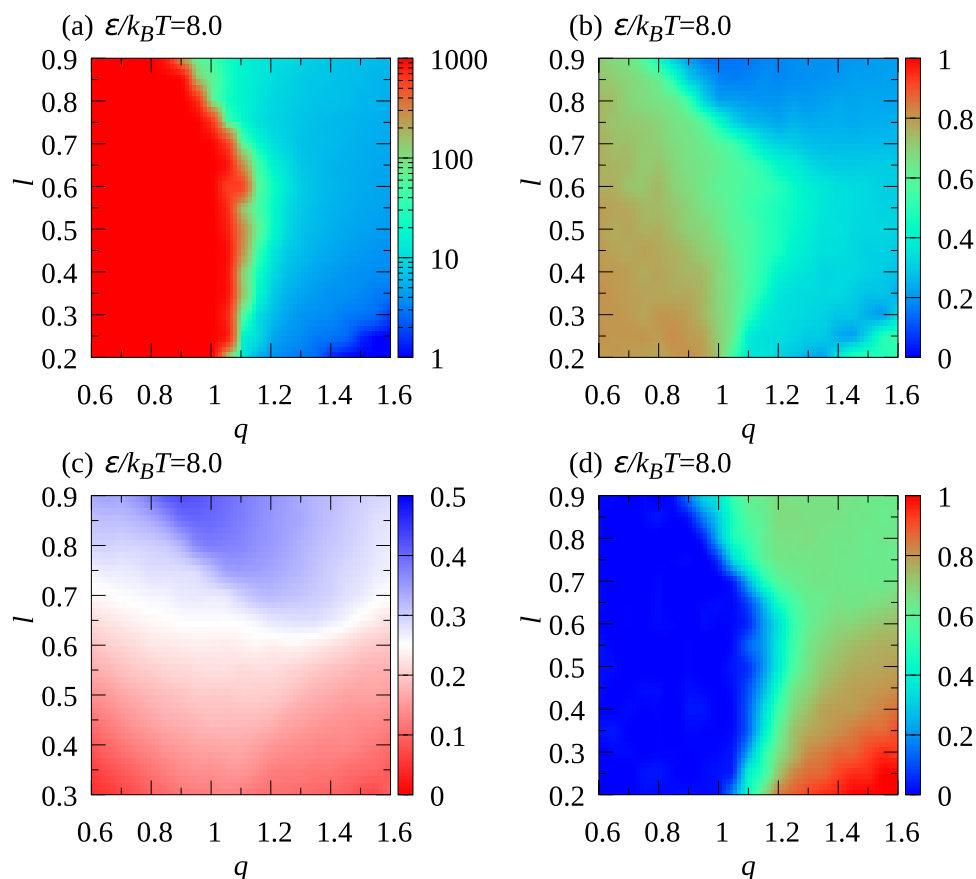


Figure 6. Dependence of (a) P_s , (b) P_z , (c) σ_z , (d) \mathcal{M} on q and l for $\epsilon/k_B T = 8.0$. (e) Top and (f) side views, and (g) top view of a double chain-like structure formed by two single chain-like clusters.

Structure and cluster shape	P_s	P_z	σ_z	\mathcal{M}
Two-dimensional island-like cluster	$> P_{s,c}$	$> P_{z,c}$	-	-
Two-dimensional chain-like cluster	$> P_{s,c}$	$< P_{z,c}$	-	-
Two-dimensional regular cluster	$< P_{s,c}$	$< P_{z,c}$	$< \sigma_{z,c}$	$< \mathcal{M}_c$
Two-dimensional elongated cluster	$< P_{s,c}$	$< P_{z,c}$	$< \sigma_{z,c}$	$> \mathcal{M}_c$
Three-dimensional elongated cluster	$< P_{s,c}$	$< P_{z,c}$	$> \sigma_{z,c}$	$> \mathcal{M}_c$

Table 1. Parameter values used to classify cluster types are $P_{s,c} = 100$, $P_{z,c} = 0.65$, $\sigma_{z,c} = 0.25$, and $\mathcal{M}_c = 0.8$.

move toward small q . Therefore, two-dimensional elongated clusters are created more readily with increasing temperature. The dependence of cluster shapes on ρ is also shown in Fig. 7c. When ρ becomes lower than that in Fig. 7a, the parameter regimes with small clusters hardly change, but the parameter regime with island-like clusters decreases by spreading the parameter regime with two-dimensional chain-like clusters.

Summary

I performed isothermal-isochoric Monte Carlo simulations in which two parameters l and q were controlled and results were analyzed to determine the types of clusters formed in thin systems. With $q \leq 1$, satisfying that the radius of the attractive area is larger than that of the non-attractive area in the dumbbell-like one-patch particles, large island-like clusters were created. Voids were frequently created in island-like clusters when \hat{n} is restricted in the two-dimensional systems⁴⁴. However, the formation of voids in island-like clusters was avoided in thin systems because the three-dimensional rotation of dumbbell-like patchy particles is allowed and \hat{n} orientate normal to the flat plane.

With L_z set slightly longer than the long axis of the dumbbell-like patchy particles, the formation of large three-dimensional chain-like cluster seemed possible if l was sufficiently large and \hat{n} aligned with the xy -plane. However, they did not form and three-dimensional elongated cluster formed instead, probably because of thermal

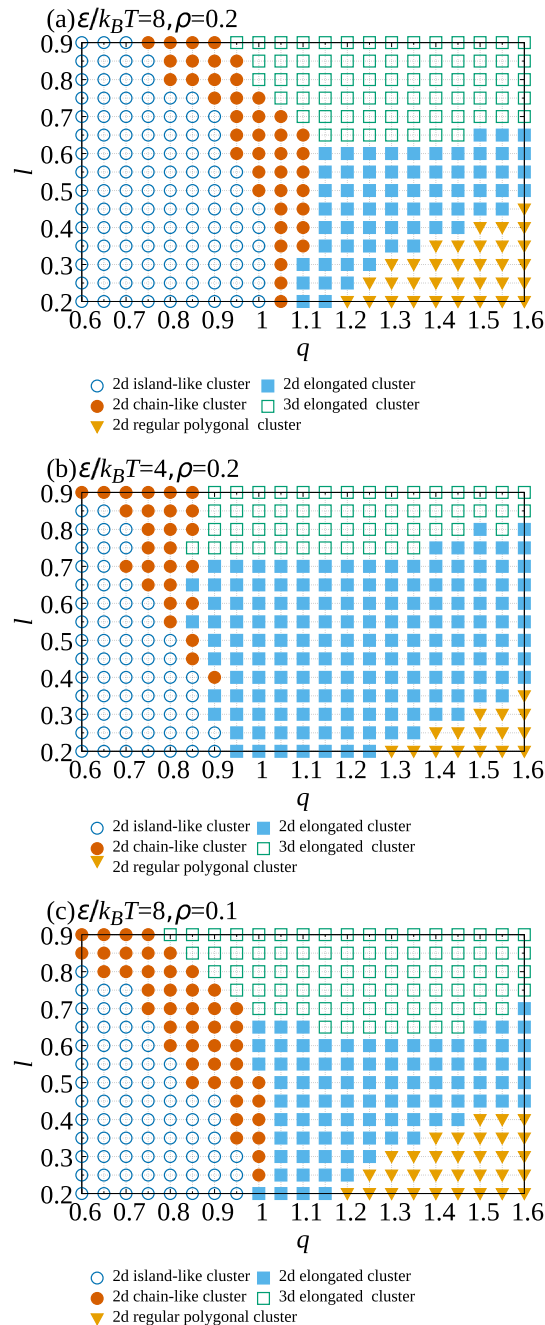


Figure 7. Dependence of cluster type on q and l for $(\epsilon/k_B T, \rho) =$ (a) (8.0, 0.2), (b) (4.0, 0.2), and (c) (8.0, 0.1).

fluctuations. If the temperature is set lower, three-dimensional chain-like clusters may be created because the energy of three-dimensional chain-like clusters is the same as that of island-like clusters.

The significant difference between spherical patchy particles and the dumbbell-like patchy particles is remarkable in the parameter regime with elongated clusters. In the two-dimensional systems with spherical patchy particles, the unit of elongated clusters is a triangular trimer. The elongated clusters are created by the connection of the triangular trimers^{7,9,10}. In the three-dimensional systems, large polyhedral clusters such as tetrahedral cluster and octahedral cluster are created^{1,4,47}. However, in the systems with dumbbell-like patchy particles, because the shape of particles is isotropic, elongated clusters are more irregular than those observed in the systems with spherical patchy particles, and large polyhedral clusters are not created in the three-dimensional systems.

In our simulations, a triangular lattice was created in island-like clusters because the interaction length was set short, whereas in a previous study the lattice in island-like clusters was square⁴⁴. The difference in interaction length affected the regular polygonal clusters. When the interaction length was long, regular square clusters were created because the particles in the diagonal positions can interact with each other. However, square clusters were not created and rhomboidal clusters formed because the interaction length was sufficiently short. Because the

systems were very thin, the cluster types were restricted in the simulations. If the system width were wider^{41,47} clusters and structures which were not observed may be created.

Methods

In my isothermal-isochoric Monte Carlo simulations, the interaction potential between two dumbbell-like particles is the modified Kern-Frenkel potential^{42–44}. For the i -th and j -th particles, the potential is expressed as $U_{ij} = U^{\text{att}} + U^{\text{rep}}$, U^{rep} being the hard-core repulsive interaction preventing pairs of particles from overlapping, and U^{att} an attractive potential given by^{42–44} $U^{\text{att}} = U^{\text{SW}}(r_{ij})f(\hat{\mathbf{r}}_{ij}, \hat{\mathbf{n}}_i, \hat{\mathbf{n}}_j)$. $r_{ij} = |\mathbf{r}_{1,j} - \mathbf{r}_{1,i}|$, $\hat{\mathbf{n}}_i = (\mathbf{r}_{1,i} - \mathbf{r}_{2,i})/d$, and $\hat{\mathbf{r}}_{ij} = \mathbf{r}_{ij}/r_{ij}$, where $\mathbf{r}_{1,i}$ and $\mathbf{r}_{2,i}$ denote the positions of the centers of the attractive and non-interactive spheres in the i -th dumbbell-like particle, respectively. $U^{\text{SW}}(r_{ij})$ is the square-well potential defined as

$$U^{\text{SW}}(r_{ij}) = \begin{cases} -\epsilon & (\sigma_1 \leq r_{ij} \leq \sigma_1 + \Delta) \\ 0 & (\sigma_1 + \Delta < r_{ij}) \end{cases}, \quad (1)$$

where ϵ is the interaction energy and Δ is the interaction length. Although Δ was set to $\sigma_1/2$ in previous studies^{42–44}, here Δ is set to $\sigma_1/10$ to ensure the interaction length is smaller than the particle size as indicated from several experiments^{7,9}. In U^{att} , $f(\hat{\mathbf{r}}_{ij}, \hat{\mathbf{n}}_i, \hat{\mathbf{n}}_j)$ represents the anisotropy in the attractive interaction, which is given by

$$f(\hat{\mathbf{r}}_{ij}, \hat{\mathbf{n}}_i, \hat{\mathbf{n}}_j) = \begin{cases} 1 & (\hat{\mathbf{n}}_i \cdot \hat{\mathbf{r}}_{ij} > \cos \delta \text{ and } \hat{\mathbf{n}}_j \cdot \hat{\mathbf{r}}_{ij} > \cos \delta) \\ 0 & \text{otherwise} \end{cases}. \quad (2)$$

Initially, the dumbbell-like particles are put in the system at random and moved without the attractive interaction 10^3 times for each particle. Then, adding the attractive interaction, rotation and translation trials were performed 2×10^6 times per particle. The maximum values for the rotation angle and translation distance in a Monte Carlo trial were tuned every $10^2 N$ trials to avoid success rates in the Monte Carlo trials begin too low⁴³; here, N is the number of particles.

Received: 3 August 2021; Accepted: 26 August 2021

Published online: 10 September 2021

References

- Hong, L., Cacciuto, A., Luijten, E. & Granick, S. Clusters of amphiphilic colloidal spheres. *Langmuir* **24**, 621–625 (2008).
- Pawar, A. B. & Kretzschmar, I. Patchy particles by glancing angle deposition. *Langmuir* **24**, 355–358 (2008).
- Chen, Q., Bae, S. C. & Granick, S. Directed self-assembly of a colloidal kagome lattice. *Nature* **469**, 381–384 (2011).
- Chen, Q. *et al.* Supracolloidal reaction kinetics of Janus spheres. *Science* **311**, 199–202 (2011).
- Chen, Q., Yan, J., Zhang, J., Bae, S. C. & Granick, S. Janus and multiblock colloidal particles. *Langmuir* **28**, 13555–13561 (2012).
- Wang, Y. *et al.* Colloids with valence and specific directional bonding. *Nature* **491**, 51–55 (2012).
- Iwashita, Y. & Kimura, Y. Stable cluster phase of Janus particles in two dimensions. *Soft Matter* **9**, 10694–10698 (2013).
- Mao, X., Chen, Q. & Granick, S. Entropy favours open colloidal lattices. *Nat. Mater.* **12**, 217–222 (2013).
- Iwashita, Y. & Kimura, Y. Orientational order of one-patch colloidal particles in two dimensions. *Soft Matter* **10**, 7170–7181 (2014).
- Iwashita, Y. & Kimura, Y. Spatial confinement governs orientational order in patchy particles. *Sci. Rep.* **6**, 27599 (2016).
- Shah, A. A., Schultz, B., Kohlstedt, K. L., Glotzer, S. C. & Solomon, M. J. Synthesis, assembly, and image analysis of spheroidal patchy particles. *Langmuir* **29**, 4688–4696 (2017).
- Gong, Z., Hueckel, T., Yi, G.-R. & Sacanna, S. Patchy particles made by colloidal fusion. *Nature* **550**, 234–238 (2017).
- Zhang, J., Grzybowski, B. A. & Granick, S. Janus particle synthesis, assembly, and application. *Langmuir* **33**, 6964–6977 (2017).
- Bianchi, E., van Oostrum, P. D. J., Likos, C. N. & Kahl, G. Inverse patchy colloids: Synthesis, modeling and self-organization. *Curr. Opin. Colloid Interface Sci.* **30**, 8–15 (2017).
- Iwashita, Y. & Kimura, Y. Density dependence of orientational order in one-patch particles. *Soft Matter* **13**, 4997–5007 (2017).
- Ravaine, S. & Dugué, E. Synthesis and assembly of patchy particles: Recent progress and future prospects. *Curr. Opin. Colloid Interface Sci.* **30**, 45–53 (2017).
- Jalilvand, Z., Pawar, A. B. & Kretzschmar, I. Experimental study of the motion of patchy particle swimmers near a wall. *Langmuir* **34**, 15593–15599 (2018).
- Noguchi, T. G., Iwashita, Y. & Kimura, Y. Controlled armoring of metal surfaces with metallodielectric patchy particles. *J. Chem. Phys.* **150**, 174903 (2019).
- Oh, J. S., Lee, S., Glotzer, S. C., Yi, G.-R. & Pine, D. J. Colloidal fibers and rings by cooperative assembly. *Nat. Commun.* **10**, 3936 (2019).
- Oh, J. S., Yi, G.-R. & Pine, D. J. Photo-printing of faceted DNA patchy particles. *Proc. Natl. Acad. Sci. U.S.A.* **117**, 10645–10653 (2020).
- Oh, J. S., Yi, G.-R. & Pine, D. J. Reconfigurable transitions between one- and two-dimensional structures with bifunctional DNA-coated Janus colloids. *ACS Nano* **14**, 15786–15792 (2020).
- Kamp, M. *et al.* Multivalent patchy colloids for quantitative 3D self-assembly studies. *Langmuir* **36**, 2403–2418 (2020).
- Morphew, D., Shaw, J., Avins, C. & Chakrabarti, D. Programming hierarchical self-assembly of patchy particles into colloidal crystals via colloidal molecules. *ACS Nano* **14**, 2355–2364 (2018).
- Rao, A. B. *et al.* Leveraging hierarchical self-assembly pathways for realizing colloidal photonic crystals. *ACS Nano* **14**, 5348–5359 (2020).
- Ho, K. M., Chan, C. T. & Soukoulis, C. M. Existence of a photonic gap in periodic dielectric structures. *Phys. Rev. Lett.* **65**, 3152–3155 (1990).
- Maldovan, M. & Thomas, E. L. Diamond-structured photonic crystals. *Nat. Mater.* **3**, 593–600 (2004).
- Shin, H. & Schweizer, K. S. Theory of two-dimensional self-assembly of Janus colloids: crystallization and orientational ordering. *Soft Matter* **10**, 262–274 (2014).
- Miller, W. L. & Cacciuto, A. Hierarchical self-assembly of asymmetric amphiphatic spherical colloidal particles. *Phys. Rev. E* **80**, 021404 (2009).
- Sciortino, F., Giacometti, A. & Pastore, G. Phase diagram of Janus particles. *Phys. Rev. Lett.* **103**, 237801 (2009).

30. Romano, F., Sanz, E., Tartaglia, P. & Sciortino, F. Phase diagram of trivalent and pentavalent patchy particles. *J. Phys. Condens. Matter* **24**, 064113 (2012).
31. Romano, F. & Sciortino, F. Patterning symmetry in the rational design of colloidal crystals. *Nat. Commun.* **3**, 975 (2012).
32. Preisler, Z., Vissers, T., Smalenburg, F., Munaò, G. & Sciortino, F. Phase diagram of one-patch colloids forming tubes and lamellae. *J. Phys. Chem. B* **117**, 9540–9547 (2013).
33. Vissers, T., Preisler, Z., Smalenburg, F., Dijkstra, M. & Sciortino, F. Predicting crystals of Janus colloids. *J. Chem. Phys.* **138**, 164505 (2013).
34. Vissers, T., Smalenburg, F., Munaò, G., Preisler, Z. & Sciortino, F. Cooperative polymerization of one-patch colloids. *J. Chem. Phys.* **140**, 144902 (2014).
35. Preisler, Z., Vissers, T., Munaò, G., Smalenburg, F. & Sciortino, F. Equilibrium phases of one-patch colloids with short-range attractions. *Soft Matter* **10**, 5121–5128 (2014).
36. Preisler, Z., Vissers, T., Smalenburg, F. & Sciortino, F. Crystals of Janus colloids at various interaction ranges. *J. Chem. Phys.* **145**, 064513 (2016).
37. Reinhart, W. F. & Panagiotopoulos, A. Z. Equilibrium crystal phases of triblock Janus colloids. *J. Chem. Phys.* **145**, 094505 (2016).
38. Patra, N. & Tkachenko, A. V. Layer-by-layer assembly of patchy particles as a route to nontrivial structures. *Phys. Rev. E* **96**, 022601 (2017).
39. Reinhart, W. F. & Panagiotopoulos, A. Z. Directed assembly of photonic crystals through simple substrate patterning. *J. Chem. Phys.* **150**, 014503 (2019).
40. Cerbelaud, M. *et al.* Brownian dynamics simulations of one-patch inverse patchy particles. *Phys. Chem. Chem. Phys.* **21**, 23447–23458 (2019).
41. Baran, Ł., Borówko, M. & Rzyśko, W. Self-assembly of amphiphilic Janus particles confined between two solid surfaces. *J. Phys. Chem. C* **124**, 17556–17565 (2020).
42. Avvisati, G., Vissers, T. & Dijkstra, M. Self-assembly of patchy colloidal dumbbells. *J. Chem. Phys.* **142**, 084905 (2015).
43. Avvisati, G. & Dijkstra, M. Phase separation and self-assembly in a fluid of Mickey Mouse particles. *Soft Matter* **11**, 8432 (2015).
44. Nakamura, K. & Sato, M. Self-Assembly of two-dimensional patchy colloidal dumbbells. *J. Phys. Soc. Jpn.* **87**, 064601 (2018).
45. Kern, N. & Frenkel, D. Fluid-fluid coexistence in colloidal systems with short-ranged strongly directional attraction. *J. Chem. Phys.* **118**, 9882 (2003).
46. Sato, M. Self-assembly formed by spherical patchy particles with long-range attraction. *J. Phys. Soc. Jpn.* **88**, 104801 (2003).
47. Sato, M. Effect of patch area and interaction length on clusters and structures formed by one-patch particles in thin systems ACS. *Omega* **5**, 28812–28822 (2020).
48. Sato, M. Effect of the interaction length on clusters formed by spherical one-patch particles on flat planes. *Langmuir* **37**, 4213–4221 (2021).
49. van Blaaderen, A., Ruel, R. & Wiltzius, P. Template-directed colloidal crystallization. *Nature* **385**, 321–324 (1997).
50. Lin, K.-H. *et al.* Entropically driven colloidal crystallization on patterned surfaces. *Phys. Rev. Lett.* **85**, 1770 (2000).
51. Savage, J. R. *et al.* Entropy-driven crystal formation on highly strained substrates. *Proc. Natl. Acad. Sci. U. S. A.* **110**, 9301–9304 (2013).
52. Dong, R., Zhang, T. & Feng, X. 2D nanomaterials: Beyond graphene and transition metal dichalcogenides. *Chem. Rev.* **118**, 6189–6235 (2018).
53. Wang, H. *et al.* Porous two-dimensional materials for photocatalytic and electrocatalytic applications. *Matter* **2**, 1377–1413 (2020).

Acknowledgements

This work was supported by JSPS KAKENHI, Grant JP20K03782 and 21K04908, and the Grant for Joint Research Program of the Institute of Low Temperature Science, Hokkaido University, Grant 21G021. I thank Richard Haase, PhD, from Edanz (<https://jp.edanz.com/ac>) for editing a draft of this manuscript.

Author contributions

M. S. performed all the simulations and analyzed the results.

Competing interests

The author declares no competing interests.

Additional information

Correspondence and requests for materials should be addressed to M.S.

Reprints and permissions information is available at www.nature.com/reprints.

Publisher's note Springer Nature remains neutral with regard to jurisdictional claims in published maps and institutional affiliations.



Open Access This article is licensed under a Creative Commons Attribution 4.0 International License, which permits use, sharing, adaptation, distribution and reproduction in any medium or format, as long as you give appropriate credit to the original author(s) and the source, provide a link to the Creative Commons licence, and indicate if changes were made. The images or other third party material in this article are included in the article's Creative Commons licence, unless indicated otherwise in a credit line to the material. If material is not included in the article's Creative Commons licence and your intended use is not permitted by statutory regulation or exceeds the permitted use, you will need to obtain permission directly from the copyright holder. To view a copy of this licence, visit <http://creativecommons.org/licenses/by/4.0/>.

© The Author(s) 2021